Multidisciplinary Applications of Detached-Eddy Simulation to Separated Flows at High Reynolds Numbers (Challenge 92)

Scott A. Morton
USAF Academy
Scott.Morton@usafa.af.mil

James R. Forsythe
Cobalt Solutions, LLC
Air Force Reserves/AFRL
forsythe@cobaltcfd.com

Russell M. Cummings
California Polytechnic State University
Russell.Cummings@usafa.edu

Kyle D. Squires
Arizona State University
squires@asu.edu

Denis B. Kholodar
USAF Academy
Denis.kholodar@usafa.af.mil

Thomas Billingsley
USAF Academy
C04Thomas.Billingsley@usafa.af.mil

Kenneth E. Wurtzler
Cobalt Solutions, LLC
wurtzler@cobaltcfd.com

Philippe R. Spalart
Boeing Commercial Airplanes
Philippe.r.Spalart@boeing.com

Abstract

The current effort develops and demonstrates the application of high resolution turbulence modeling to flight mechanics and aeroelasticity of air vehicles at flight conditions where the vehicle is experiencing massively separated flow fields. The effort has both a basic research component to aid in developing the method and an applied component where the method is used to demonstrate an ability to simulate current DoD aircraft issues in flight mechanics and aeroelasticity. The high resolution turbulence method is a hybrid Reynolds Averaged Navier-Stokes (RANS)-Large Eddy-Simulation (LES) method introduced by Spalart et. al. in 1997 called Detached-Eddy Simulation (DES) implemented in an unstructured Navier-Stokes solver, *Cobalt*.

In the basic research component, DES has been applied to an Aerospatiale-A airfoil at an angle of attack of 13.3 degrees and a Reynolds number of 2 million. The project is called DESFOIL and simulates laminar-to-turbulent transition, adverse pressure gradients, streamline curvature, and boundary layer separation of a 3-D airfoil strip. This study is in the early stages of developing a baseline for RANS and DES computations.

DES has also been applied to flight mechanic and aeroelasticity problems of DoD air vehicles to demonstrate the utility of DES and also discover some of the nonlinear mechanisms causing these flight issues. The applications studied include the F/A-18E forced motion about the roll axis and one degree of freedom simulation of abrupt wing stall (AWS), the F/A-18C at conditions of tail buffet, the CV-22 Tilt Rotor aircraft in a vortex ring state (VRS), and the ARGUS missile at conditions where it experiences coning motion.

1 Introduction

This work focuses on multidisciplinary applications of Detached-Eddy Simulation (DES), principally flight mechanics and aeroelasticity. Specifically, the lateral instability (known as abrupt wing stall) of the pre-production F/A-18E is reproduced using DES, including the unsteady shock motion. A single degree-of-freedom calculation is performed as well to demonstrate the onset of the wing drop. DES is applied to the F/A-18C at a moderate angle of attack to reproduce the vortex breakdown leading to vertical stabilizer buffet. Unsteady tail loads are compared to flight test data.

Previous DoD Challenge work has demonstrated the unique ability of the DES turbulence treatment to accurately and efficiently predict flows with massive separation at flight Reynolds numbers. DES predictions are obtained on unstructured grids using the *Cobalt* code, an approach that can accommodate complete configurations with very few compromises. A broad range of flows has been examined in previous Challenge work, including aircraft forebodies, airfoil sections, a missile afterbody, vortex breakdown on a delta wing, and the F-16 and F-15E at high angles-of-attack. All DES predictions exhibited a moderate to significant improvement over results obtained using traditional Reynolds-averaged models and often excellent agreement with experimental/flight-test data is observed. DES combines the efficiency of a Reynolds-averaged turbulence model near the wall with the fidelity of Large-Eddy Simulation (LES) in separated regions. The development and demonstration of improved methods for the prediction of flight mechanics and aeroelasticity in this Challenge is expected to reduce the acquisition cost of future military aircraft.

The F/A-18E flight mechanic simulations are in the second full year of development. The previous year, static calculations were made of a full and half span model at conditions where it experiences AWS. These simulations compared very favorably with experimental data. This year's effort incorporated dynamic motion of the vehicle along the roll axis to mimic wind tunnel free-to-roll experiments. Two different pitch angles were examined and unsteady data was obtained and compared to the experimentally obtained frequency data. The current calculations have so far qualitatively captured the experimental data. This application has made great strides in demonstrating the utility of using an unstructured solver and DES to compute the critical nonlinear aerodynamics necessary to estimate static and dynamic control derivatives of fighter aircraft.

The F/A-18C tail buffet calculations are also in the second year of development. Simulations were performed on a configuration similar to the F-18 High Alpha Research Vehicle and compared to flight test data.

2 Numerical Method

Solutions were computed with the commercial version of *Cobalt* developed by Cobalt Solutions.[1] *Cobalt* solves the unsteady, three-dimensional, compressible Navier-Stokes equations on a hybrid unstructured grid. The code has several choices of turbulence models, including Spalart Almaras (SA), and Menter's Shear Stress Transport (SST) RANS, as well as DES versions of SA and SST. All simulations were computed on unstructured meshes with prisms in the boundary layer and tetrahedra elsewhere on half-span surface geometries. The computational meshes were generated with the software packages GridTool[2] and VGRIDns.[3]

For simulation of turbulent flows, the governing equations are suitably averaged, yielding turbulent stresses that require a model. A Boussinesq approximation is invoked in the momentum equations and the turbulent eddy viscosity (μ_t) is used to relate the stresses to the strain rate. The turbulent heat flux is also modeled using a gradient-transport hypothesis, requiring specification of a turbulent thermal conductivity, k_t. The Reynolds analogy is applied and the turbulent heat flux is modeled using a constant turbulent Prandtl number of 0.9. Using turbulent eddy viscosity and turbulent conductivity, the variable μ is replaced by $(\mu + \mu_t)$ and k is replaced by $(k + k_t)$ in the governing equations.

Detached-Eddy Simulation (DES) was proposed by Spalart et al.[4,5] The motivation for this approach was to combine large-eddy simulation (LES) with the best features of Reynolds-averaged Navier-Stokes (RANS) methods. RANS methods have demonstrated an ability to predict attached flows very well with a relatively low computational cost. LES methods have demonstrated an ability to compute seperated flowfields accurately, but at a tremendous cost for configurations with boundary layers. Spalart's DES method is a hybrid of LES and RANS, which combines the strengths of both methods.

The DES model was originally based on the Spalart-Allmaras one equation RANS turbulence model. The wall destruction term is proportional to $(\tilde{\nu} / d)^2$, where d is the distance to the wall. When this term is balanced with the production term, the eddy viscosity becomes proportional to $\hat{S}d^2$ where $\hat{S}$ is the local strain rate. The Smagorinski LES model varies its sub-grid scale (SGS) turbulent viscosity with the local strain rate, and the grid spacing: $\nu_{SGS} \propto \hat{S}\Delta^2$, where $\Delta = \max(\Delta x, \Delta y, \Delta z)$. If d is replaced with Δ in the wall destruction term, the S-A model will act as a Smagorinski LES model.

To exhibit both RANS and LES behavior, d in the SA model is replaced by

$$\tilde{d} = \min(d, C_{DES}\Delta).$$

When $d << \Delta$, the model acts in a RANS mode and when $d >> \Delta$ the model acts in a Smagorinski LES mode. Therefore the model switches into LES mode when the grid is locally refined.

DES was implemented in an unstructured grid method by Forsythe et al.[6] They determined the C_{DES} constant should be 0.65, consistent with the structured grid implementation of Spalart et al.[4] when the grid spacing Δ was taken to be the longest distance between the cell center and all of the neighboring cell centers.

A Newton sub-iteration method is used in the solution of the system of equations to improve time accuracy of the point-implicit method and approximate Jacobians. In the calculations presented below, a typical number of three Newton sub-iterations is used for all time-accurate cases.

2.1 Summary of the Proposed Method

The proposed method for simulating aircraft at flight Reynolds numbers in conditions of massively separated flow is as follows:

1. Use a time-accurate unstructured-grid solver with moving mesh capability to allow rapid turn around of grids on complex configurations -- the solution must have at least second-order spatial and temporal accuracy.
2. Use DES as the underlying turbulence treatment to obtain accurate unsteady loads and mean quantities – this requires a low dissipation solver.
3. Use Adaptive Mesh Refinement (AMR) to improve grid resolution in critical areas with nonlinear flowfield phenomena.

3 Results

Results are shown for both the basic and applied portions of the challenge project. The basic project is a start-up effort to investigate laminar to turbulent transition on an airfoil shape. In the applied portion of the study two full aircraft configurations are analyzed for flight mechanic and aeroelastic phenomena of abrupt wing stall and tail buffet and then two configurations are analyzed as a result of flight test support requests.

DESFOIL

Prediction of complex flows that include laminar-to-turbulent transition, adverse pressure gradient, streamline curvature, and boundary layer separation remain among the most challenging for turbulence simulation strategies. A prototypical example that is the focus of the present investigation is the flow over an airfoil at maximum lift. Flow regimes are sensitive to the airfoil geometry, angle of attack, and Reynolds number and motivate various hierarchies of simulation strategies. The specific flow of interest is that over the Aerospatiale-A airfoil at an angle of attack of 13.3 degrees and Reynolds number of 2 x 10^6, corresponding to maximum lift. The flow has been measured in separate experiments and was the subject of an coordinated set of investigations through the LESFOIL project.

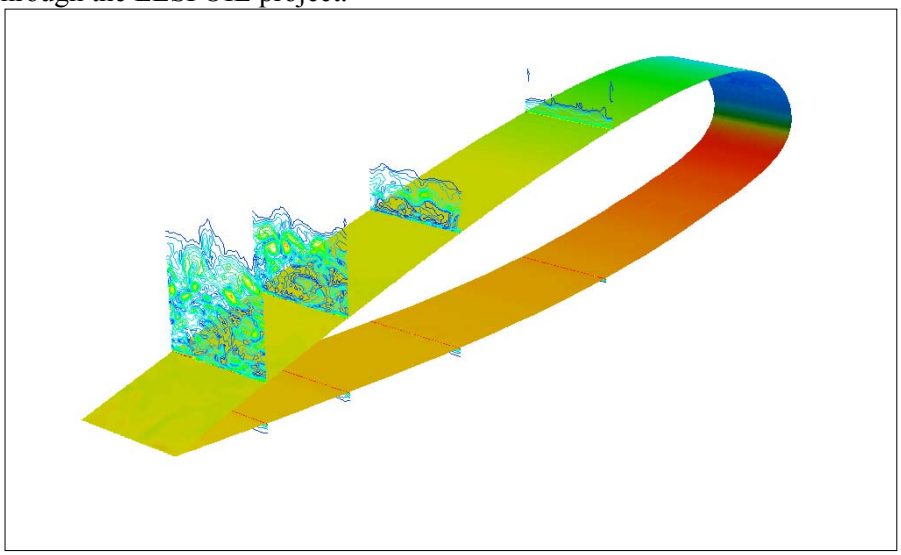

Figure 1: Contours of instantaneous vorticity in four planes along the Aerospatiale-A airfoil at an angle of attack of 13.3 degrees and a Reynolds number of 2 X 10^6.

DES and Reynolds-averaged Navier-Stokes predictions have been obtained of the flow over the airfoil, with the objectives to date being to establish a baseline upon which enhancements to the predictive technique can be assessed. Shown in Fig. 1 are contours of the instantaneous vorticity in four planes along the airfoil. At x/C = 0.4, the RANS model is retained and the figure illustrates that the solution possesses weak spanwise variation. At the subsequent planes a range of scales is resolved as the flow develops eddies in the separating shear layer. The computations performed to date have successfully demonstrated the approach of handling laminar-to-turbulent transition is numerically feasible and relatively accurate. Further investigations will begin the process of incorporating eddy-seeding strategies into the simulations, along with substantial grid refinement in order to support turbulent structures within the boundary layer in the aft region of the airfoil. There remain very significant challenges to the modeling strategy that will require substantial computational resources, in turn further motivating the need for HPC resources.

F/A-18E Abrupt Wing Stall

During envelope expansion flights of the F/A-18E in the Engineering and Manufacturing Development phase, the aircraft encountered uncommanded lateral activity, which was labeled "wing drop". An extensive resolution process was undertaken to resolve this issue. A production solution was developed, which included revising the flight control laws and the incorporation of a porous wing fold fairing to eliminate the wing drop tendencies of the pre-production F/A-18E/F. The wing drop events were traced to an abrupt wing stall (AWS) on one side of the wing causing a sudden and severe roll-off in the direction of the stalled wing. Development of a reliable computational tool for prediction of abrupt wing stall would enable designers to screen configurations prior to building the first prototype, reducing costs and limiting risks.

The F/A-18E provides an excellent testing ground for simulation tools due to the large amount of experimental data obtained.[7,8] Previous computational research[9] focused on predicting the zero sideslip characteristics of the aircraft, including the break in the lift curve slope characteristic of AWS. It was found that by applying Detached-Eddy Simulation (DES) to this problem to predict the unsteady shock motion seen experimentally, a better mean flow prediction could be obtained compared to industry standard Reynolds-averaged (RANS) models.[10]

The current work seeks to extend the past computational successes to predicting stability derivatives (both static and dynamic) in the AWS regime. An unstructured full aircraft grid was created with 8.4×10^6 cells by using a coarse baseline grid and then using solution based mesh adaptation to cluster points in the separation region above the wing. Both Menter's SST RANS model and Detached-Eddy Simulation were applied. To assess the accuracy of the simulations, comparisons are made against experiments. Normal force vs. angle of attack is plotted in Figure 2, showing the slope break in the experiments. DES shows a better agreement than SST RANS in this case, as was seen in previous work.

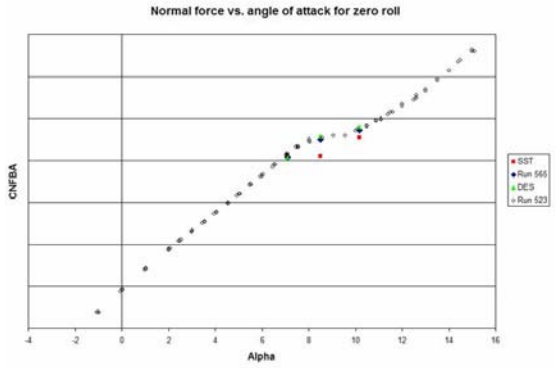

Figure 2: Normal force vs. angle of attack for near zero sideslip for the F/A-18E at M=0.9.

Calculations were also performed with various bank and pitch angles. For the experiments and computations, the pitch angle was held fixed, and the model rolled around the longitudinal axis of the aircraft. This leads to a reduction in alpha, and an increase in beta. Thus the calculations do not strictly give derivatives with respect to beta. Figure 3 shows rolling moment and yawing moment vs. roll angle for 7° pitch angle. The agreement to experiments for yawing moment is quite good, since this comes mainly from the vertical stabilizer, which is not separated. The agreement for rolling moment is less accurate since the unsteady location of the shock, which separates the flow on the wing, is challenging to predict. The change in sign in rolling moment for the SST RANS at 30° bank was due to the shock on the down-turned wing moving forward, decreasing lift on that wing.

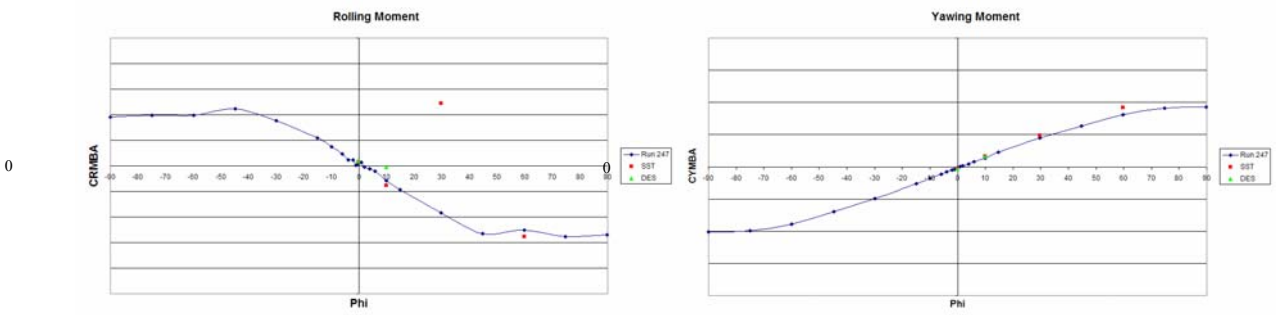

Figure 3: Rolling moment (left) and yawing moment (right) vs. bank angle for the F/A-18E at 7° pitch angle

Calculations have also been performed in a forced oscillation to estimate roll damping. A sample flow visualization from a DES simulation illustrating the separated region is shown in Figure 4. Also shown for the DES simulation are phase averaged plots for four pitch angles, each derived from five cycles of the rolling moment vs. non-dimensionalized roll rate. Stable behavior (i.e., negative slope) is seen at 6° and 7°. At 8° there are some strong non-linearites, while the 9° plot shows regions of unstable roll damping.

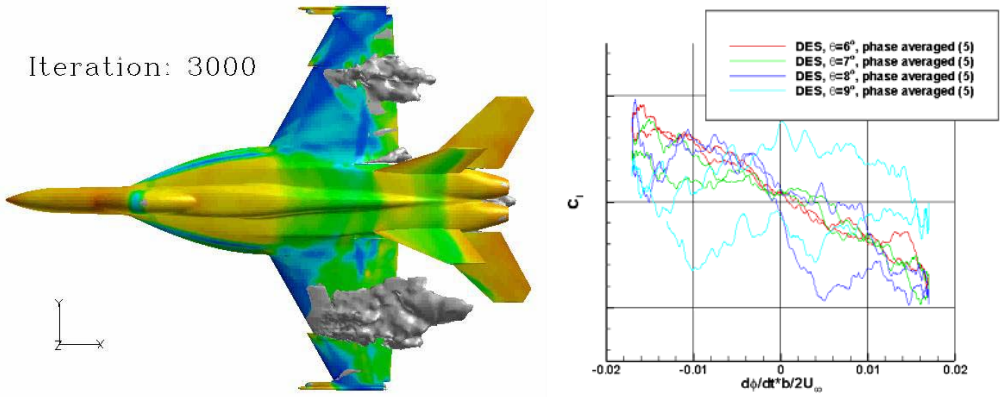

Figure 4: DES forced oscillations simulations. Left pane, instantaneous flow visualization at 6° pitch angle - contours of pressure on surface, and isosurface of zero streamwise velocity (grey). Right pane, rolling moment vs. roll rate phase averaged over 5 cycles.

Clearly, the ability to computationally predict static and dynamic stability, especially at transonic and higher Mach numbers, where experimental facilities are quite limited, would provide a significant increase in capability for airplane design and analysis. Free-to-roll computations are currently underway to compare directly to free-to-roll experiments, which have been highly successful in correlating to flight tests.

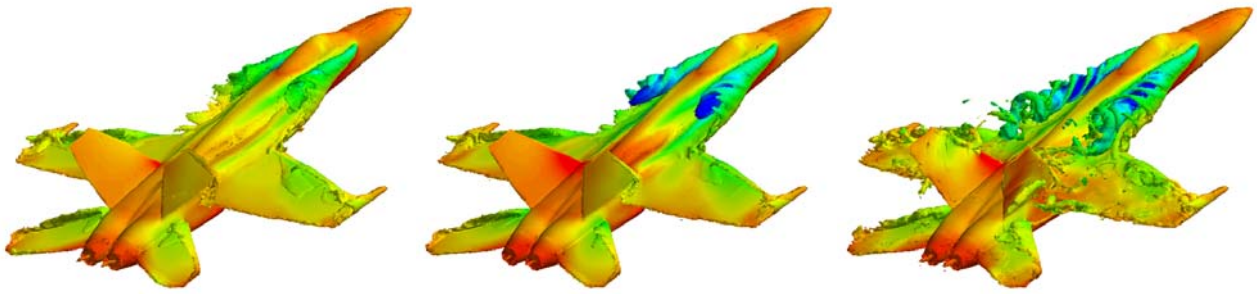

a) SST b) SA c) SADES

Figure 5. Isometric views of the F/A-18C at $\alpha = 30°$, $Re_c = 13 \times 10^6$, leading edge flaps set to -33°, trailing edge flaps set to 0°, with no diverter slot present: a) SST turbulence model, b) SA turbulence model, and c) SADES turbulence model.

F/A-18C Tail Buffet

The F/A-18C simulations were conducted to demonstrate the ability of the method to reproduce the aerodynamics of tail buffet. Tail buffet of the F/A-18C is a fluid structure interaction resulting from burst leading-edge extension vortices impacting the twin vertical tails and was observed in extensive flight tests of the F-18 HARV. At realistic flight conditions this flow field is also complicated by turbulent flow generated in the post breakdown region surrounding the tails and in the boundary layer of the vehicle. Results are compared to unsteady tail pressure coefficient data and vortex breakdown locations obtained in the NASA F-18 HARV flight tests. Follow-on studies of this configuration will incorporate aeroelastic tails to fully simulate the phenomena.

All F/A-18C cases were run at 30° angle-of-attack, a Mach number of 0.2755, and a standard day altitude of 20,000 feet. The resulting Reynold's number was 13 million based on the mean aerodynamic chord of the aircraft (12 ft). The baseline grid of 3.6 million cells was generated with

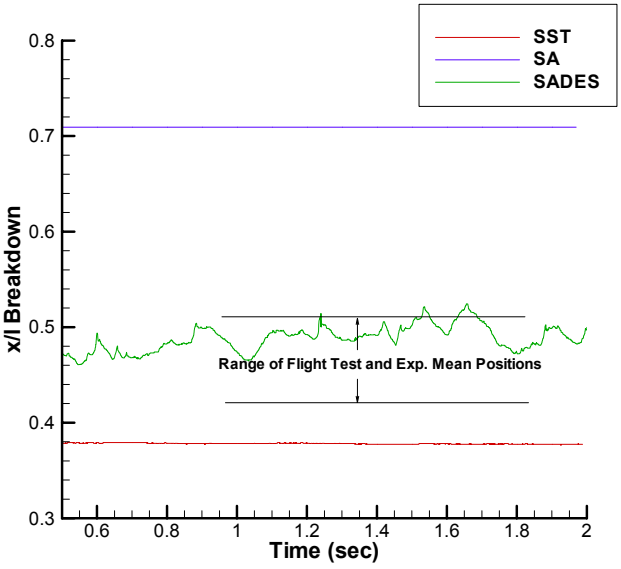

Figure 6. Time histories of the streamwise coordinate of vortex breakdown referenced to the vehicles nose and scaled by the length for the SST, SA, and SADES methods.

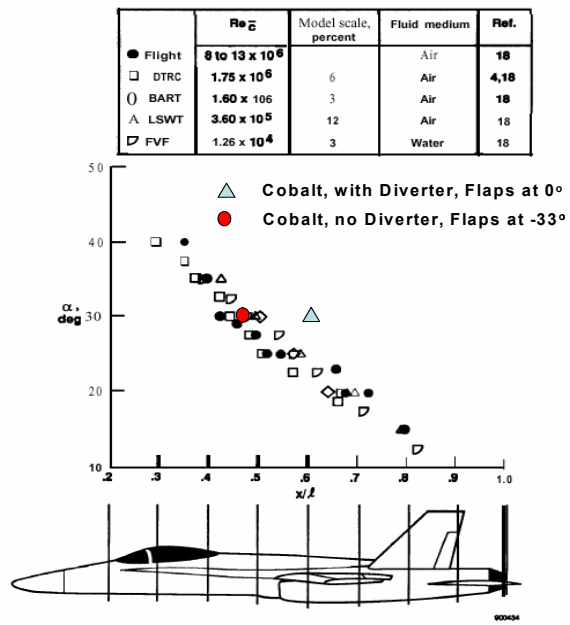

Figure 7. Streamwise LEX vortex breakdown position as a function of angle of attack, extracted from Ref. 47 SADES mean vortex breakdown position in red.

VGRIDns. Unsteady SADES turbulence model simulations were performed using the baseline grid. A time-averaged SADES solution was used to produce an AMR grid with 3.9 million cells by following the approach outlined in Ref. 44. All time-accurate simulations were run for over 10,000 iterations with second-order temporal and spatial accuracy, three Newton sub-iterations, and a time step of 0.0005 seconds. The chosen time step results in a time step non-dimensionalized by the freestream velocity and mean aerodynamic chord of 0.0012. This characteristic time step was found adequate in previous studies of vortex breakdown and massively separated flows.[11,12,13,14]

Solutions were computed using the SST, SA, and SADES turbulence models to determine their effect on the flowfield. Solutions for all three methods were computed using the same grid, time step, and number of sub-iterations to provide a consistent comparison. Figure 5 a-c depicts snapshots of solutions for each method with the surface colored by pressure and an iso-surface of vorticity shown. The chosen vorticity level for the isosurface and the pressure colormap are held fixed. Although the snapshots are not necessarily synchronized in time, the overall differences are striking. The SADES solution (Fig. 5c) produces a much more detailed view of the simulation since it is able to capture much finer flowfield scales. The SST (Fig. 5a) and SA (Fig. 5b) models are unable to capture the proper post-breakdown behavior or the leading-edge separation regions of the wing, horizontal, and vertical tails. It is also apparent that the SST LEX vortex pressure footprint on the surface is significantly different than either the SA or SADES solutions. The low pressure region represented by a dark green color is greatly reduced in size on the SST solution. The SADES solution is also capturing the vortical sub-structures around the primary vortex.

A common definition of vortex breakdown is the location where the streamwise velocity component is zero in the core. The coordinates of this point along the core were tracked in time for each of the methods, SST, SA, and SADES. Figure 6 depicts the time histories of the three methods as well as the flight test and experiment maximum and minimum mean values of vortex breakdown presented in Ref. 15. Three things are obvious from Fig. 6. First, the amplitude of oscillation for the SST and SA models is almost negligible compared to the SADES simulation. Second, the SST solution predicts breakdown far upstream of the flight test or experimental values whereas the SA solution predicts the breakdown location downstream of the flight test and experimental results. Third, the SADES solution gives a mean value of vortex breakdown location well within the flight test and experimental data. It should also be noted that the computed nondimensional primary frequency of the breakdown oscillation is 0.2 in the range of frequencies commonly found in the literature[16] for vortex breakdown. This inability of commonly used turbulence models to accurately compute a solution with breakdown is well documented in the literature and is due to the large amount of eddy-viscosity these models put into the core of vortices. Several researchers have proposed fixes to these turbulence models by incorporating some form of a rotation correction. The disadvantage of this approach is the fact the simulation will still be operating in a RANS mode and compute solutions that are relatively steady post-breakdown as opposed to an LES approach that resolves the eddies that produce the unsteadiness. It is clear in Fig's 5 and 6 that the SADES method does not suffer from the same problem as the RANS methods due to the fact that eddy viscosity is computed based on sub-grid scale turbulence, automatically minimizing the amount of spurious eddy-viscosity that is placed in the core of vortices.

Figure 7 is a well known plot in the literature of the streamwise location of the LEX vortex breakdown as a function of angle-of-attack[15]. The current solutions fall in the range of flight tests and experiments plotted at 30^{o} angle of attack. The previous comparisons of the method with the flight test and experimental data was poor due to the incorrect flap settings and diverter slot being uncovered.[13]

This section presents comparison of the computed SADES solutions with F-18 HARV flight test data from NASA Dryden. The HARV was instrumented with 32 kulite pressure sensors, half on the inboard and half on the outboard sections of the right vertical tail (Fig. 8). The kulite pressures were stored every 30ms as a function of time. The available pressures were stored relative to a reference pressure that is unfortunately unknown. The lack of known reference pressures allowed only frequency comparisons rather than frequency and amplitude comparisons of the SADES data with flight test data. Pressure ports of Fig. 8 circled in red are those used for comparison with the SADES simulations.

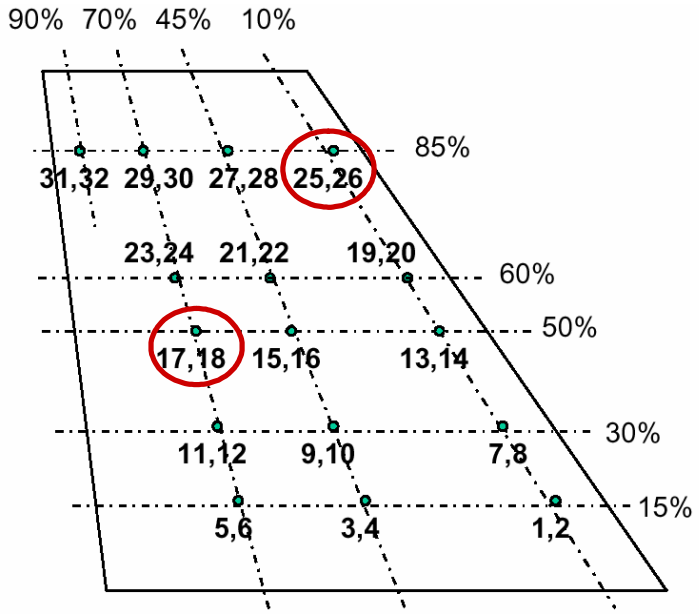

Figure 8. Placement of the F-18 HARV Kulite pressure sensors on the right vertical tail.[47] Odd port numbers are on the inboard section of the tail and even are on the outboard section. Red circles around ports indicates those used in comparing flight test to SADES.

The flight test and SADES simulation port pressures were analyzed with MATLAB's PSD function. Since the flight test data has a different time step and period of time (40 sec), the power resulting from a PSD analysis will not be a one to one match but the frequencies and characteristic shapes of the PSD should match. All 32 pressure ports were analyzed but only a representative set are shown. Figures 9 a-b depict the comparison of SADES and flight test data. Figure 14a shows the PSD data for flight test and SADES simulation for ports 17 and 18, and 9b shows ports 25 and 26. In all cases, the frequency content shows quite good comparison between the flight test and SADES simulations. All of the ports show a wide peak amplitude range corresponding to Strouhal numbers between 0.45 and 0.8 for both flight test and SADES simulations. This frequency range corresponds to pressure sweeps over the tail surface observed in a movie clip of the SADES simulation. Unfortunately, the published first bending mode is at a Strouhal number of approximately 0.66 explaining why the tail is so aeroelastically active at this flight condition. Most of the ports also show matches in slopes of the PSD for the Strouhal range of 1 – 10. It is also interesting to note that when the flight test curves for each port lie on top of each other this is true for the SADES solutions as well (Figs. 9a and b), and when the flight test curves are separated they are separated by approximately the same amount in the SADES solutions (Fig. 9b). A consistency is noted in the level of power between inboard and outboard ports for both flight test and SADES, i.e. when the inboard port has a higher power for flight test that is true as well for the SADES simulation. Finally, when the curves cross, this occurs at approximately the same frequency for flight test and SADES (Fig. 9b). The overall comparison of frequency content is remarkably good for the SADES solutions, demonstrating the utility of the method for tail buffet computations at flight Reynolds numbers.

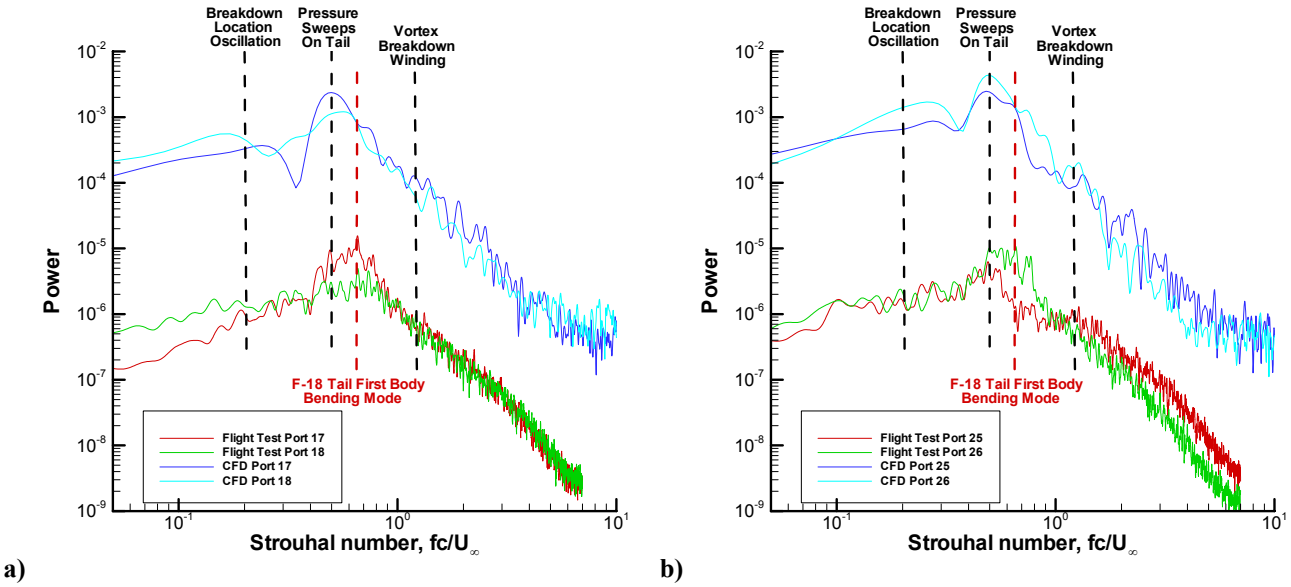

Figure 9. Comparison of Power Spectrum Density from Flight Test and DES Prediction for a) Ports 17 & 18, and b) Ports 25 & 26.

The final two configurations analyzed were in direct response to DoD customer requests to help in understanding the nonlinear aerodynamics causing undesirable flight mechanics of current vehicles in flight test programs. These two applications are the CV-22 experiencing VRS and the ARGUS missile experiencing coning after release. In both cases simulations have compared favorably with experiments and a greater understanding of the undesirable phenomena has been obtained. The CV-22 VRS simulations will continue in the follow-on years with a more sophisticated unsteady blade element model of the rotors and a six degree of freedom simulation of the vehicle in VRS is anticipated. The ARGUS missile simulations are preliminary to six degree of freedom simulations of the free flight of the missile following release.

V-22 Vortex Ring State

DES calculations were performed on the V-22 and isolated rotors (i.e. no aircraft) with the same size and spacing as the V-22 rotors. Calculations were performed with a symmetry plane, and the full configuration (both left and right hand sides) and using an actuator disk model with a uniform (ideal) thrust distribution specified. A refined grid (medium) of $7.7X10^6$ cells for the V-22 was also run with cell sizes a square root of 2 smaller than the baseline grid (coarse) of $3.2X10^6$ cells.

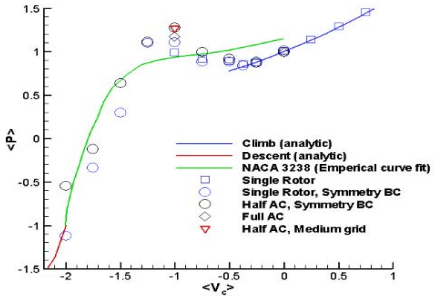

Figure 10: Time-averaged induced power as a function of the vertical velocity for a single rotor with/without a symmetric boundary condition, and a V-22 half aircraft and full V-22 aircraft.

Power was calculated by integrating the downward component of velocity times the thrust per unit area over the rotor and taking a time average. The resulting power for all runs is plotted in Fig. 10 against non-dimensional climb rate (non-dimensionalized by the ideal downwash velocity in hover, negative velocities correspond to descents). There is good agreement for the climb and slow descent rate to the analytical curve based on momentum theory[17]. The power begins to increase below a climb rate of -0.5, an indicator of vortex ring state (VRS). The emperical curve is shown from Ref. 17 for comparison in the VRS range. Note that the power is higher for this curve even in hover, since this curve is from experiments with non-ideal thrust distributions. Reference 17 was a curve fit from several experiments which contained a significant amount of scatter (not shown). The DES calculations fall within this scatter and seem to provide a reasonable description of the onset of VRS. However, a one-to-one comparison to exisiting VRS experiments of an isolated tilt-rotor need to be performed to increase the confidence of the predictive capability[18]. Given the crudeness of the rotor model, the current results are quite encouraging.

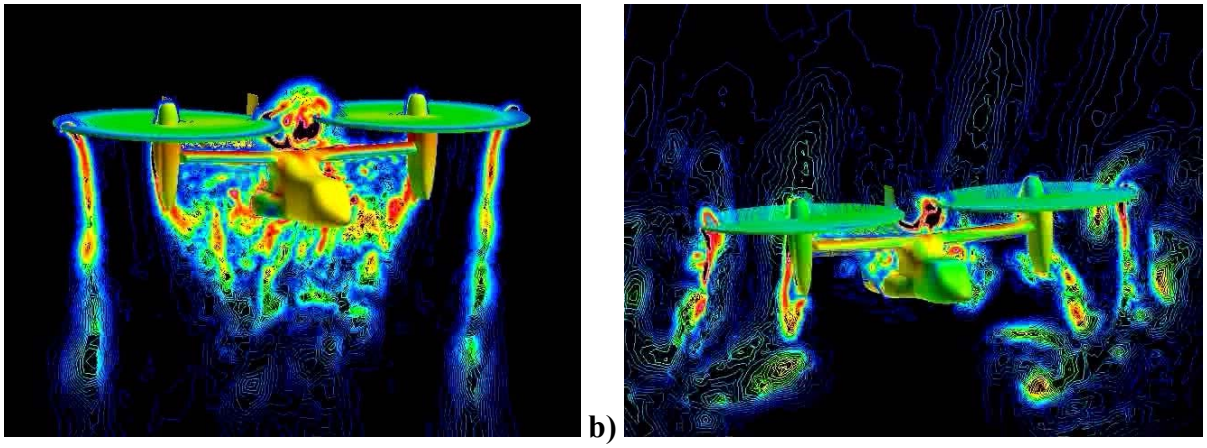

a) b)

Figure 11: a) Instantaneous cross-plane of vorticity contours for the V-22 in hover. b) Instantaneous cross-plane of vorticity contours for the V-22 in a descent.

Fig. 11 a and b depict results of the full aircraft medium grid ($7.7X10^6$ cells) in hover and in a descent. The hover case (Fig. 11a) shows an instantaneous cross-sectional plane of vorticity at a longitudinal station through the center of the rotor hubs. The vorticity contours indicate massive separation below the wing with significant unsteadiness but the outboard tips of the rotors produce fairly symmetric structures. A descent rate is depicted in Fig. 11b, a condition consistent with vortex ring state in Fig. 10. It is evident that the vortical structures at the tips of the rotors are very asymmetric. These vortical structures produce unsteadiness in the aircraft loads due to the moment arm to the center of the aircraft. It is important to note that this condition is outside of the V-22's operational envelope and is only computed to gain an understanding of the VRS phenomenon. The DES method is necessary for accurate computation of this flowfield due to the large eddy content away from the vehicle surface and the importance of the boundary layer at the surface.

ARGUS

The ARGUS program is intended to meet the Air Force requirement of detecting, tracking, identifying and reporting Time Sensitive Targets in near real time. The first generation version of ARGUS (Steel Eagle II) had an asymmetric geometry which resulted in undesirable stability characteristics. A newly designed ARGUS projectile was recently created by Textron, Inc. to achieve improved aerodynamic characteristics. To complement the development effort, CFD analysis of the new design is being conducted by the Academy's Department of Aeronautics to determine the projectile's lift, drag, and aerodynamic moment characteristics. Problems that were encountered with the previous Steel Eagle II design included instability in the sensor air

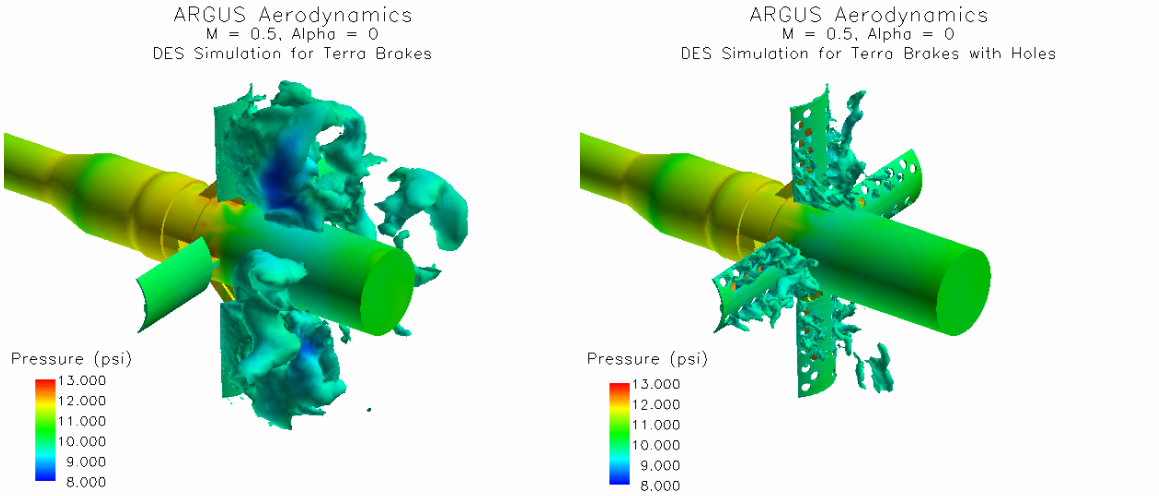

Figure 12: Iso-surfaces of vorticity for the ARGUS simulations for terra brakes with and without holes at a Mach number of 0.5 and an angle of attack of 0 degrees.

body when deployed from a carrier aircraft or helicopter, coning instability during free flight, non-zero impact angles, and high impact velocities.

Most of the problems mentioned above relate to the coning motion of the vehicle. While it was apparent that the vehicle displayed coning in flight, neither flight testing nor wind tunnel testing could fully discover why the motion was taking place. Detached-Eddy Simulation (DES) of the flow field for the ARGUS geometry was conducted at $M = 0.5$ and $\alpha = 0°$ and vortex shedding was detected from the terra brakes. Researchers at USAFA suggested that the vortex shedding could be alleviated by drilling holes into the terra brakes, so a DES simulation of that configuration was also conducted at the same flight conditions. While the flow field behind the terra brakes with holes is still unsteady, all evidence of vortex shedding is gone—the resulting lateral forces and moments have shown a corresponding reduction due to the addition of the brakes, which should alleviate the coning problem. Initial drop tests from a helicopter have verified these results, and the ARGUS geometry will be designed with holes in the terra brakes.

3 Conclusions

The proposed method of solution was used in both basic and applied simulations in the Challenge C92 project during FY 04. The basic research effort made preliminary progress in broadening the application of the method to laminar-turbulent transition and embedded LES. The applications made great strides towards aiding flight test of full aircraft in the most difficult portions of their operational envelopes. The F/A-18E and F/A-18C showed excellent comparison with experiment and flight tests lending credibility to the method. In addition, the method was used to aid in two current DoD flight test programs, CV-22 and ARGUS, by helping to understand complex nonlinear aerodynamics observed in flight test and experiment resulting from massively separated flow. In the case of the ARGUS missile system the simulations resulted in a design change of the vehicle.

References

[1] Strang, W.Z., Tomaro, R.F., Grismer, M.J., "The Defining Methods of Cobalt: A Parallel, Implicit, Unstructured Euler/Navier-Stokes Flow Solver," AIAA Paper 99-0786, Jan. 1999.

[2] Samareh, J., "Gridtool: A Surface Modeling and Grid Generation Tool," Proceedings of the Workshop on Surface Modeling, Grid Generation, and Related Issues in CFD Solution, NASA CP-3291, 1995.

[3] Pirzadeh, S., "Progress Toward A User-Oriented Unstructured Viscous Grid Generator," AIAA Paper 96-0031, Jan. 1996.

[4] Spalart, P. R. , Jou W-H. , Strelets M. , and Allmaras, S. R., "Comments on the Feasibility of LES for Wings, and on a Hybrid RANS/LES Approach," *Advances in DNS/LES, 1st AFOSR Int. Conf. on DNS/LE*S, Aug. 4-8, 1997, Greyden Press, Columbus Oh.

[5] Strelets, M., "Detached-Eddy Simulation of Massively Separated Flows," *AIAA 01-0879*, Jan 2001.

[6] Forsythe, J.R., Hoffmann, K.A., Dieteker, F.F., "Detached-Eddy Simulation of a Supersonic Axisymmetric Base Flow with an Unstructured Flow Solver," AIAA Paper 2000-2410, June 2000.

[7] Lamar, J., Hall, R., "AWS Figures of Merit Developed Parameters from Static Transonic Model Tests," *AIAA 03-0745*, Jan 2003.

[8] Owens, B., Brandon, J., Capone, F., Hall, R., Cunningham, K., "Free-to-Roll Analysis of Abrupt Wing Stall on Military Aircraft at Transonic Speeds," *AIAA 03-0750*, Jan 2003.

[9] Woodson, S.H., Green, B.E., Chung, J.J., Grove, D.V., Parikh, P.C., Forsythe, J.R., "Recommendations for CFD Procedures for Predicting Abrupt Wing Stall," *AIAA 2003-0923*, Jan 2003.

[10] Forsythe, J.R., Woodson, S.H., "Unsteady CFD Calculations of Abrupt Wing Stall using Detached-Eddy Simulation," *AIAA 2003-0594*, Jan 2003.

[11] Morton, S.A., Forsythe, J.R., Mitchell, A.M., and Hajek, D., "DES and RANS Simulations of Delta Wing Vortical Flows," AIAA Paper 2002-0587, Jan. 2002.

[12] Forsythe, J.R., Squires, K.D., Wurtzler, K.E., and Spalart, P.R., "Detached-Eddy Simulation of Fighter Aircraft at High Alpha," *Journal of Aircraft*, Vol. 41, No. 2, 2004, pp. 193-200.

[13] Morton, S.A., Steenman, M.B., Cummings, R.M., and Forsythe, J.R., "DES Grid Resolution Issues for Vortical Flows on a Delta Wing and an F-18C," AIAA Paper 2003-1103, Jan. 2003.

[14] Morton, S.A., Cummings, R.M., and Kholodar, D.B., "High Resolution Turbulence Treatment of F/A-18 Tail Buffet," AIAA Paper 2004-1676, Apr. 2004.

[15] Ghaffari, F., "Navier-Stokes, Flight, and Wind Tunnel Flow Analysis for the F/A-18 Aircraft," NASA TP 3478, Dec. 1994.

[16] Gursul, I., "Review of Unsteady Vortex Flows Over Delta Wings," AIAA Paper 2003-3942, June 2003.

[17] Gessow, A., "Review of Information on Induced Flow of a Lifting Rotor," NACA Technical Note 3238, Aug 1954.

[18] Potsdam, M.A., and Strawn, R.C., "CFD Simulations of Tiltrotor Configurations in Hover," Proceedings of the 58th Annual Forum of the American Helicopter Society, June 2002.